WHISPERING GALLERY MODES IN QUANTUM DOT-EMBEDDED

DIELECTRIC MICROSPHERES FOR TAGLESS REMOTE

REFRACTOMETRIC SENSING

A Thesis

by

SHUO PANG

Submitted to the Office of Graduate Studies of
Texas A&M University
in partial fulfillment of the requirements for the degree of

MASTER OF SCIENCE

August 2008

Major Subject: Biomedical Engineering

WHISPERING GALLERY MODES IN QUANTUM DOT-EMBEDDED

DIELECTRIC MICROSPHERES FOR TAGLESS REMOTE

REFRACTOMETRIC SENSING

A Thesis

by

SHUO PANG

Submitted to the Office of Graduate Studies of
Texas A&M University
in partial fulfillment of the requirements for the degree of

MASTER OF SCIENCE

Approved by:

Chair of Committee,   Kenith E. Meissner
Committee Members,   Alvin T. Yeh
                                    Jun Kameoka
Head of Department,   Gerard L. Coté

August 2008

Major Subject: Biomedical Engineering

ABSTRACT

Whispering Gallery Modes in Quantum Dot-embedded Dielectric Microspheres for

Tagless Remote Refractometric Sensing. (August 2008)

Shuo Pang, B.E., Tsinghua University

Chair of Advisory Committee: Dr. Kenith E. Meissner

This thesis presents the development of a refractometric sensor based on quantum dot-embedded polystyrene microspheres. The technique uses optical resonances within a microsphere, known as Whispering-Gallery Modes (WGMs), which produce narrow spectral peaks. The basic theory of WGMs is reviewed and specifically discussed for biosensing application.

The spectral shifts of WGM peaks are sensitive to changes in the local refractive index. In the experiments, two-photon excited luminescence from the quantum dots couples into several WGMs within the microresonator. By optimizing the detection area, the spectral visibility of the WGMs is improved. The spectral shifts are measured as the surrounding index of refraction changes. The experimental sensitivity is about five times greater than that predicted by Mie theory.

The sensor element is based on commercially available dielectric microspheres with a diameter about 10 μm. Thus, the technique is more economic and suitable for sensing applications, compared to microspheres of 100 μm in size which can only be made in the laboratory.

DEDICATION

       To my affectionate parents for their unconditional love and support throughout my life.

ACKNOWLEDGEMENTS

I am grateful to my advisor, Dr. Kenith Meissner, who has been very supportive on guiding me through my research. The discussions between us are never limited to the experimental details—his aspiration and attitude towards research will be a priceless treasure to me. I would also like to thank my committee members, Dr. Alvin Yeh and Dr. Jun Kameoka. My special thanks to Dr. Yeh for his knowledge and insight that has always helped me to keep the big picture in mind during my research. I would like to thank Dr. Richard Beckham for his help in small particle coating and synthesis. I am also thankful to the members from our group and the Yeh Group, Hari Balasubramanian, Hope Beier, Kyle Borque, Ameet Juriani, Adam Larson, Pofeng Lee, Bhavik Nathawani, Clark Needham, and Suhani Shah, who are very friendly and helpful people.

During my study at Texas A&M University, my parents have always been encouraging. They have always been there, whenever I needed them. Finally, I would like to thank all my friends in Aggieland for their help in many aspects of my life.

TABLE OF CONTENTS

LIST OF FIGURES

LIST OF TABLES

1. INTRODUCTION:

THE IMPORTANCE OF RESEARCH

Optical microspherical cavity resonators have recently been applied in bio-sensing [1-10]. The resonance modes, known as Whispering-Gallery Modes (WGMs), arise from confinement of light within a resonant cavity through total internal reflection. The resonance shift due to local refraction index changes can detect near-surface molecules without labeling [1, 3, 4, 6-8, 10]. In most WGM sensor systems, light is coupled by intimate contact between the microresonator and an evanescent wave source, which precludes remote sensing [1-4, 6-8, 10]. Linewidth changes of WGM peaks in optically-trapped, dye-doped microspheres have also been reported as refractometric sensor [11]. However, high power optical tweezing accelerates photobleaching of the organic dye, and is unstable during fluidic change [12].

Here we demonstrate a remote refractometric sensor based on WGM shifts within a quantum dot(QD)-embedded microsphere [13, 14]. The QDs serve as a local broadband light source to couple light into the microresonator. Due to their high quantum yield and resistance to photobleaching, QDs provide a strong and stable signal. Using localized two-photon excitation, the visibility of WGMs is improved by exclusion of the excitation volume. The measured shifts due to the refractive index change of the immersion fluid show more than a five fold enhancement over the theoretical calculation for an uncoated microresonator. By averaging the relative shifts of all the modes within

_____

This thesis follows the style of Optics Express.

the QD emission spectrum, the random error can be reduced. The improved sensitivity and accuracy of WGM based refractometric sensors offer a promising opportunity for the development of remote microscale elements for biomedical and environmental applications.

2. BACKGROUND

2.1 Optical Resonance in Microcavity—Whispering Gallery Mode

Whispering Gallery Modes (WGMs) result from light confinement due to total internal reflection inside a high index spherical surface within a lower index medium and from resonance as the light travels a round trip within the cavity with phase matching [15]. The confinement enables multiple interferences and results in an extremely narrow spectral mode structure [15-17]. WGM is named after the whispering gallery at St. Paul's Cathedral in London [18].

Compared with the case for common optical fiber, in which light is confined in a cylindrical surface but not limited in the axial direction, the whispering gallery mode is confined in three dimensions. In order to determine the resonance condition, and electric and magnetic field distribution of the resonance modes, the Maxwell's equations with appropriate boundary conditions can formulate this problem [16].

The electric and magnetic field distribution of a lossless microsphere with an incident infinite plane wave has been well developed. The theory was developed in 1908 by Gustav Mie and Ludvig Lorenz, and is known as Mie Theory [16]. In Mie theory, the incident plane wave is decomposed into the sum of infinite normal modes. The normal modes satisfy Maxwell's equations and the boundary conditions. Each normal mode has characteristic mode numbers: angular mode number, l; radial mode number, i. Every normal mode, according to polarization, can be categorized into either transverse electric (TE) mode or transverse magnetic (TM) mode. In TE mode, the electric field has no

radial component, and in TM modes the magnetic field has no radial component. The scattering electric field of TE and TM mode can be expressed as:

$$\mathbf{M}_l^i(r,\theta,\phi) = \frac{\exp(jl\phi)}{kr} S_i(r)\mathbf{X}_l^i(\theta) \tag{1}$$

$$\mathbf{N}_l^i(r,\theta,\phi) = \frac{\exp(jl\phi)}{k^2 m(r)^2}\left[\frac{1}{r}\frac{dT_i(r)}{dr}\mathbf{Y}_l^i(\theta) + \frac{1}{r^2}T_i(r)\mathbf{Z}_l^i(\theta)\right] \tag{2}$$

where the function $\mathbf{M}_l^i(r,\theta,\phi)$ are TE modes and the function $\mathbf{N}_l^i(r,\theta,\phi)$ are the TM modes; $\mathbf{X}_l^i(\theta)$, $\mathbf{Y}_l^i(\theta)$, and $\mathbf{Z}_l^i(\theta)$ are the angular functions; and $S_i(r)$ and $T_i(r)$ are the radial functions. The detailed definitions can be found in Ref [15].

The incident field is decomposed into normal modes with a coefficient for each mode. According to Bohren and Huffman's denotation, the scattering field and the internal field can also be expressed as the sum of the normal modes [16]. Only the coefficients for the internal field and the scattering field are different. For convenience, only the scattering electric field is shown.

$$\mathbf{E}_{scatter} = E_0 \sum_{n=1}^{\infty} j^n \frac{2n+1}{n(n+1)}\left(ja_n\mathbf{N}_l^i(r,\theta,\varphi) - b_n\mathbf{M}_l^i(r,\theta,\varphi)\right) \tag{3}$$

a_n and b_n are the Mie scattering field expansion coefficients. A solution to this formula is found in Ref [16] with equations for the a_n and b_n coefficients:

$$a_n = \frac{m^2 j_n(mx)[xj_n(x)]' - j_n(x)[mxj_n(mx)]'}{m^2 j_n(mx)[xh_n^{(1)}(x)]' - h_n^{(1)}(x)[mxj_n(mx)]'} \tag{4a}$$

$$b_n = \frac{j_n(mx)[xj_n(x)]' - j_n(x)[mxj_n(mx)]'}{j_n(mx)[xh_n^{(1)}(x)]' - h_n^{(1)}(x)[mxj_n(mx)]'} \tag{4b}$$

where j_n is the nth spherical Bessel function of the first kind and $h_n^{(1)}$ is the nth Hankel function of the first kind, x is the size parameter defined as $x=kn_ea=2\pi n_e a/\lambda$, where a is the radius of the microspheres, and k, n_e and λ are the wave number, refractive index of the environmental medium, and the wavelength in vacuum, respectively, and n_s is the refractive index of the medium surrounding the sphere. m is defined as the relative refractive index, $m=n_s/n_e$, between the sphere and the immersion medium.

It is convenient to define the Ricatti-Bessel functions for further discussion.

$$\psi_l(x) = xj_n(x) \tag{5a}$$

$$\chi_l(x) = xy_n(x) \tag{5b}$$

$$\zeta_l(x) = \psi_n(x) + j\chi_l(x) \tag{5c}$$

The denominators of a_n and b_n thus can be expressed as:

$$m\psi_l(mx)\zeta'_l(x) - \zeta_l(x)\psi'_l(mx) \tag{6a}$$

$$\psi_l(mx)\zeta'_l(x) - m\zeta_l(x)\psi'_l(mx) \tag{6b}$$

It is natural to think that if we set (6a) to zero or make it very small then the correspondent TE mode will dominate the scattering field, and if (6b) is zero or very small then the correspondent TM mode will dominate the scattering field. In both cases, WGMs will be observed. However, it should be noted that $\zeta_l(x)$ is a complex function and only a complex size parameter will allow (6a) and (6b) equal to zero [16]. If one analyzes the total scattering efficiency field overall intensity by defining scattering efficiency as:

$$Q_{sca} = \frac{2}{x^2} \sum_{l=1}^{\infty} (2n+1)\left(|a_n|^2 + |b_n|^2\right) \tag{7}$$

Figure 1 shows the scattering efficiency as a function of the size parameter. By running the Mie code, one can observe the ripples of the scattering field.
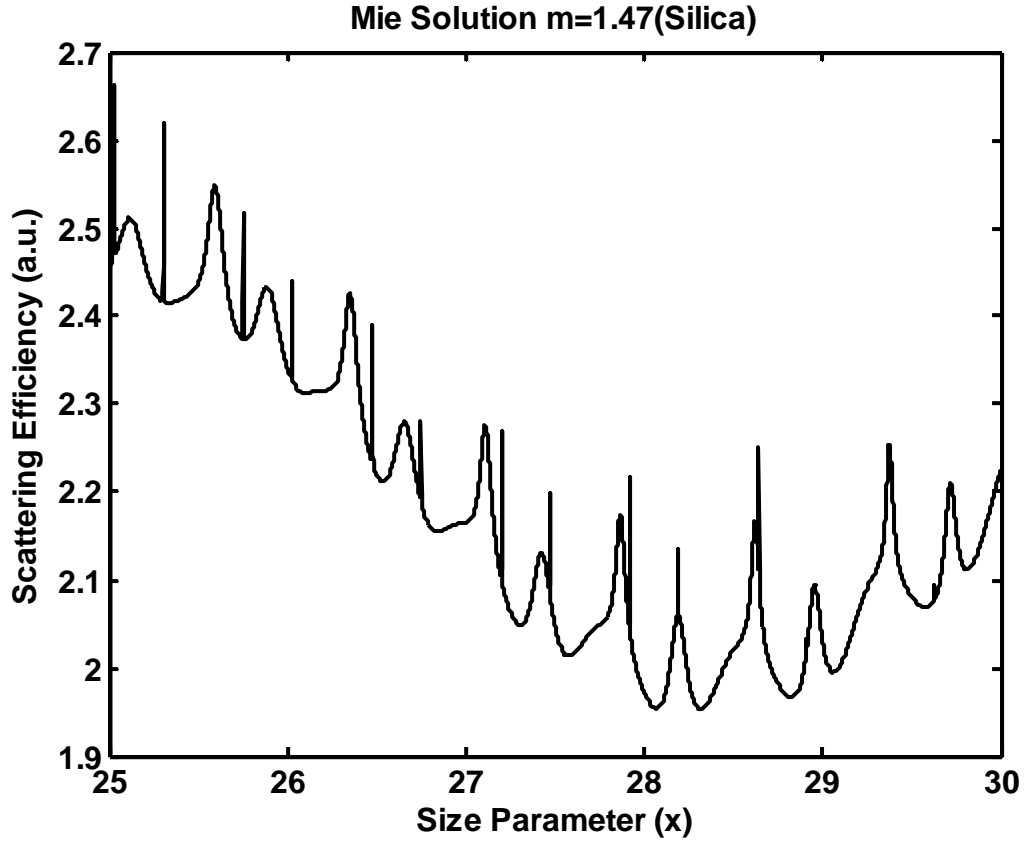
Fig. 1. Mie scattering efficiency for silica microspheres. Silica spheres ($n_s = 1.47$) in air ($n_e = 1.0$) with different size parameter; the sharp and narrow peaks are Whispering-Gallery Modes (WGMs).

The narrow ripples representing the WGMs occur when the imaginary part of one coefficient equals to zero. Though at these conditions (6a) and (6b) are not zero, the coefficient, either a_n or b_n is large enough to make one mode dominate the scattering field [16]. The size parameters of these conditions satisfy the following equations [17]:

$$\frac{\chi_l(x)}{\chi_l{}'(x)} = m\frac{\psi_l(mx)}{\psi_l{}'(mx)} \qquad (8a)$$

$$m\frac{\chi_l(x)}{\chi_l{}'(x)} = \frac{\psi_l(mx)}{\psi_l{}'(mx)} \qquad (8b)$$

A closer look at the radial function of the electric field using a quantum mechanics analogy will help develop a better understanding of the WGMs. At the size parameter satisfy either (8a) or (8b) the radial equation is [15]:

$$\frac{d^2 S_l(r)}{dr^2} + \left[k^2 m^2 - \frac{l(l+1)}{r^2} \right] S_l(r) = 0 \qquad (9)$$

Recall the one dimension Schrödinger equation:

$$-\frac{d^2\psi(r)}{dr^2} + V(r)\psi(r) = E\psi(r) \qquad (10)$$

where E is the energy and V is the potential. To illustrate the concept of confinement, it's convenient to define E and V as the following:

$$E = k^2 \qquad (11a)$$

$$V_l(r) = \begin{cases} k^2(1-m^2) + l(l+1)/r^2, \text{ for } r \leq a \\ l(l+1)/r^2, \text{ for } a < r \end{cases} \qquad (11b)$$

Equation (9) can be expressed in the form of Schrödinger equation. We examine the solution for two resonance conditions. Figure 2 shows the electric field of the light within the microresonator for a silica microsphere in air (m=1.47) of the first radial TE 40 mode, the resonance size parameter of which is 31.0589. Figure 3 shows the electric filed of the light for a silica microsphere (n_s = 1.47) in air (n_e = 1.00) of the second radial TE 40 mode, the resonance size parameter of which is 34.6112.

S(r)(m = 1.47, x = 31.0589, TE$_{40,1}$)

Fig. 2. The quantum analogy of the resonance theory (1st radial mode). The effective potential function (dashed line --) and electric field (solid line –) of first radial mode at TE 40 resonance in silica microspheres ($n_s = 1.47$) in air ($n_e = 1.0$).

The potential function V near the surface region shows a clear dip. In analogy to quantum mechanics theory, the dip serves as a potential well, and the electric field function is the wave function. The electric field is "trapped" near the surface area of the microsphere. In the area out side the sphere, (r/a > 1), which is the classic forbidden region, the electric field tunnels into the surrounding medium, but its amplitude decays evanescently.
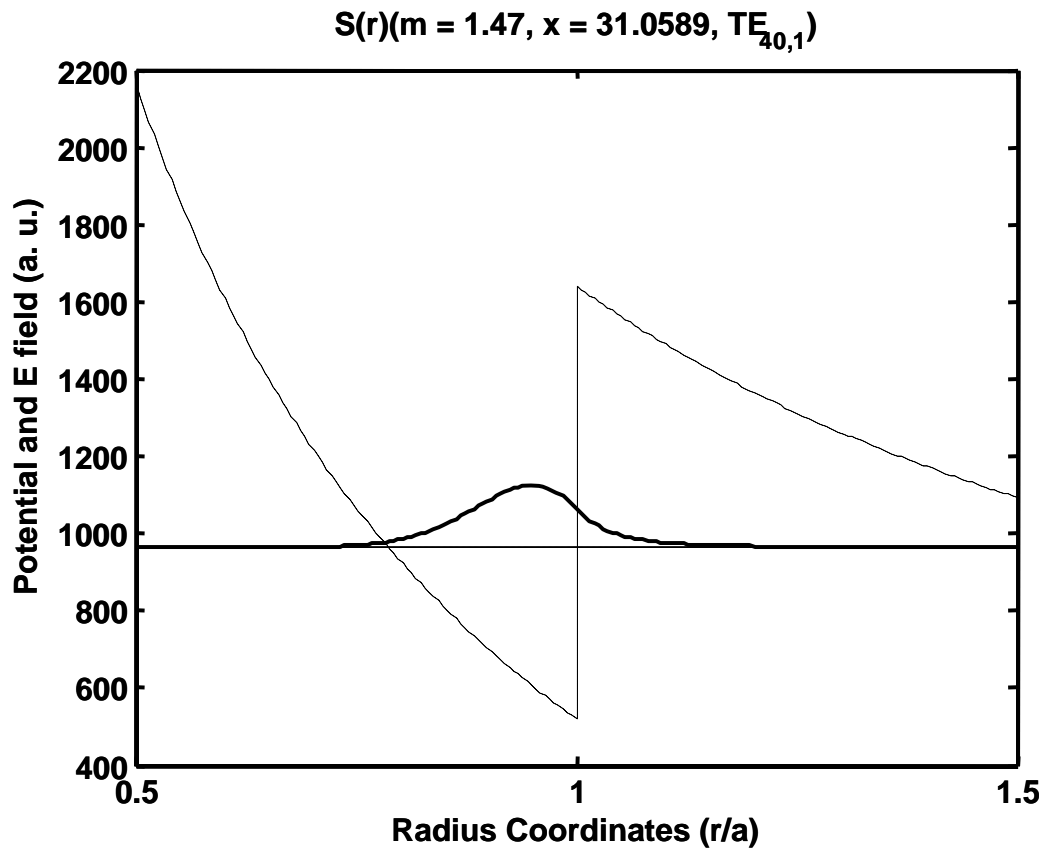
S(r)(m = 1.47, x = 34.6112, TE$_{40,2}$)
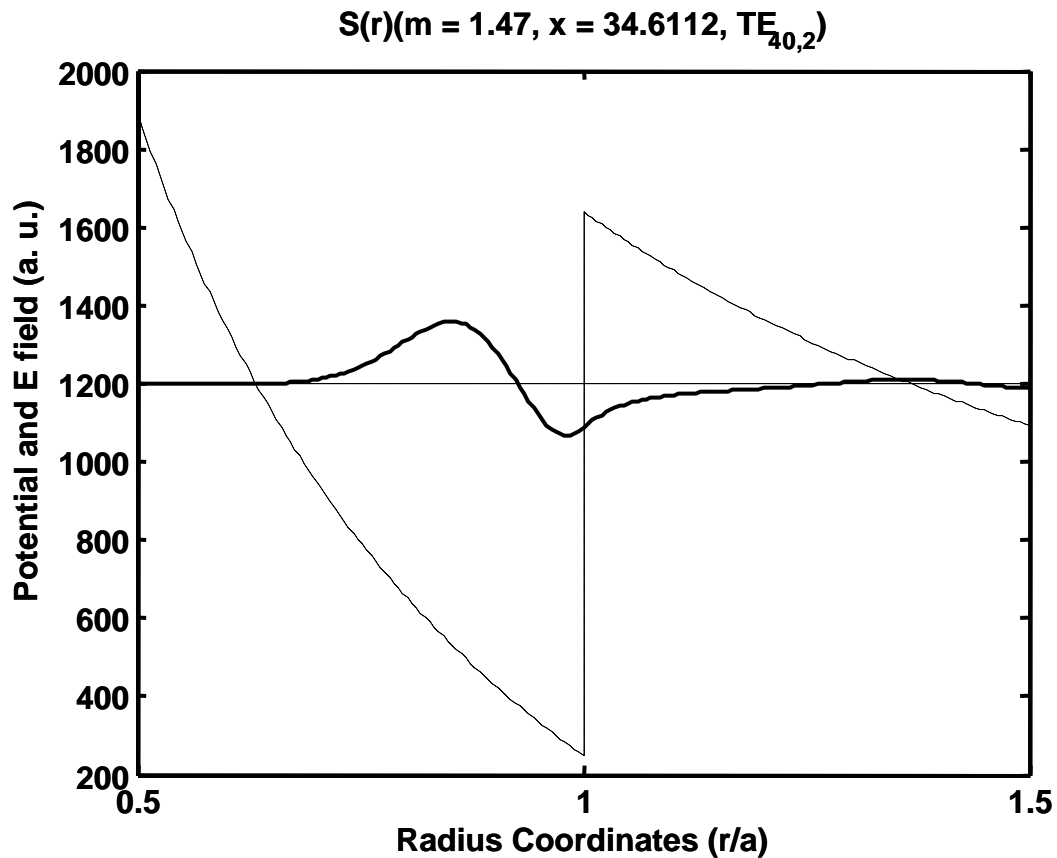
Fig. 3. The quantum analogy of the resonance theory (2nd radial mode). the effective potential function (dashed line --) and electric field (solid line –) of second radial mode at TE 40 resonance in silica microspheres (n_s = 1.47) in air (n_e = 1.0).

The second redial mode has two intensity maxima in the potential well. As in the first radial mode, the electric field also evanesces into the surrounding medium. The energy level of the second radial mode is higher than that of the first radial mode, so the confinement is less than that of the first radial mode. Thus the second radial mode induces a broader resonance width. Figure 4 and figure 5 show the resonance pattern in the horizontal plan of the first and second radial mode, respectively.

Fig. 4. WGM electric field (1st radial mode). The Mie solution of the electric field in the horizontal plane of the first radial mode at TE 40 resonance in silica microspheres ($n_s = 1.47$) in air ($n_e = 1.0$).

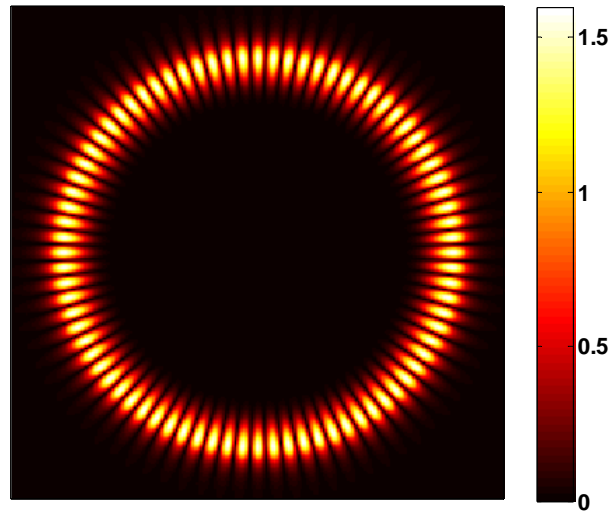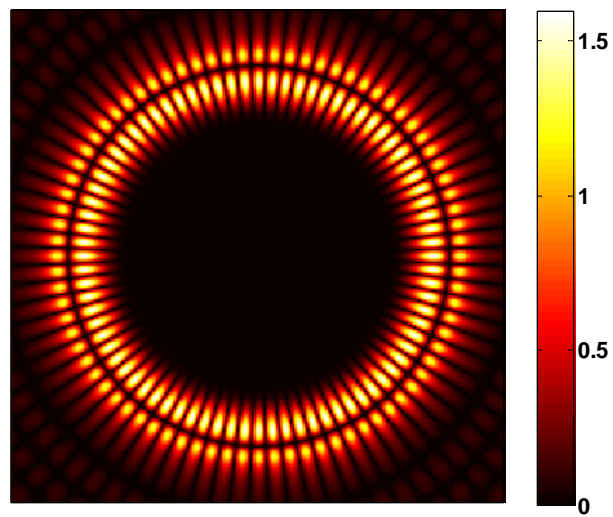Fig. 5. WGM electric field (2nd radial mode). The Mie solution of the electric field in the horizontal plane of the second radial mode at TE 40 resonance in silica microspheres ($n_s = 1.47$) in air ($n_e = 1.0$).

2.2 Whispering Gallery Mode Sensor

As described in the previous section, the WGMs have an evanescent tail that extends up to approximately 100 nm into the surrounding media. For sensing applications, the modal structure will change due to changes in the index of refraction within the volume sampled multiple times by the evanescent tail [1, 4, 6, 7, 19, 20]. The shift in the modal position and/or the modal spacing may be used for sensing the presence of an analyte near the surface of the sensing element, when the surface is bio-chemically functionalized. Figure 6 illustrates the concept of applying WGM sensor in biochemical detection.
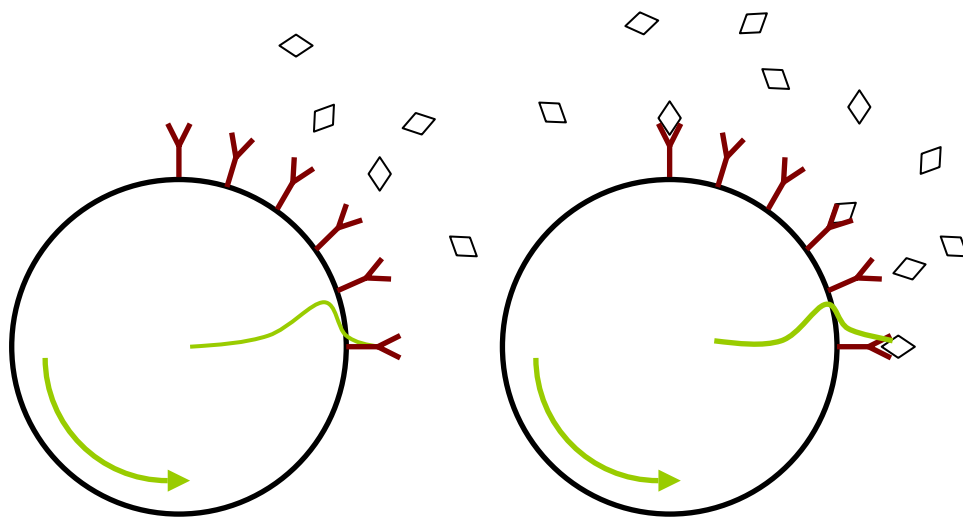
Fig. 6. Illustration of the WGM sensor. The resonance condition changes induced by binding with target analyte (shown as diamonds). The green curve represents the WGM mode inside the sphere and the evanescent tail outside the sphere. Binding process induces a change in the mode structure, and a spectral shift can be observed.

WGM resonators are an emerging bio-sensing technology that has recently been the subject of intensive research. Compared to bio-sensing techniques based on fluorescence [21, 22], WGM resonators are capable of detecting unlabeled molecules.

Recent progress in unlabeled sensing techniques has seen optics play a strong role through the use of surface plasmon resonances [23]. Turnover of the substrate by the enzyme leads to the release of a surface targeting dye serves as an amplifier to surface enhanced Raman spectroscopy (SERS). Otherwise, SERS can not detect single molecule signal [23]. Eliminating molecular labels avoids interference in sensing interactions and allows for real-time measurements [1].

Compared to other techniques without labeling such as fiber-optic wave guides [24], nanowires [25], and nanoparticle probes[26], WGM sensors sample the surrounding medium many times, so the sensitivity is superior to other techniques. Recent research reported that WGM biosensors have the ability to detect single molecules [1].

In conventional WGM sensor systems, microspheres with diameters of 50 μm or larger serves as the resonant cavities [2-4, 6-8, 10]. Light is coupled to the cavity through evanescent waves from the side of an eroded optical fiber or the end of an angle polished fiber, as shown in Figure 7. As shown in Figure 7(a), light from a tunable diode laser, the wavelength of which is usually in the infrared range, is coupled into the microsphere by total internal reflection through an angle polished fiber prism [2]. The microspheres are often made by melting the end of an optical fiber. A detector measures the scattered light from the microsphere. When a WGM resonance condition is satisfied, light is confined to the surface area of the microsphere. The detector therefore will monitor a dip of the scattering intensity. Figure 7(b) illustrates another configuration of the WGM sensor system [7]. In this setup, the tunable laser light is coupled into a

tapered fiber and then evanescently coupled into the microsphere. The detector at the end of the fiber monitors the coupling of WGMs and measures modal shifts.
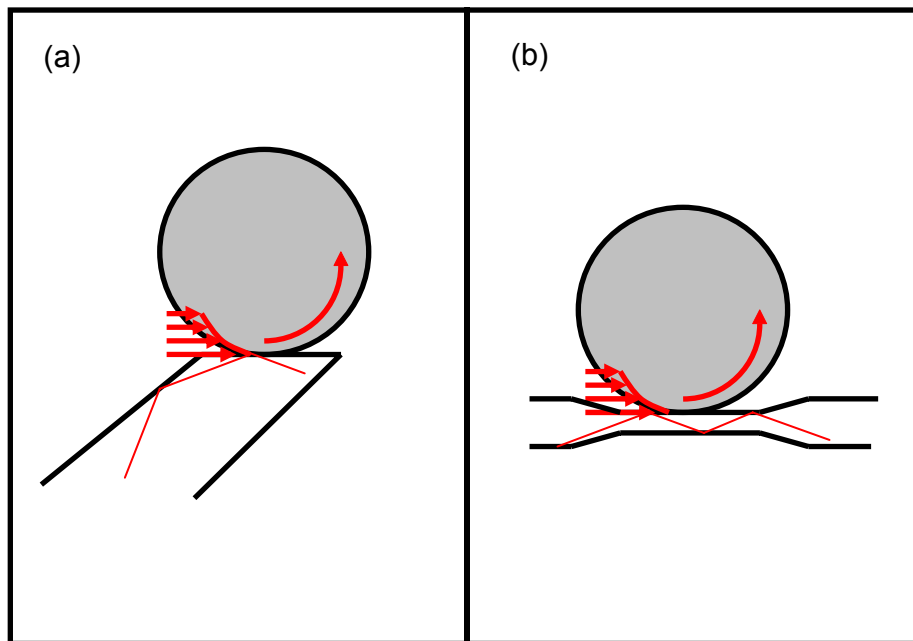
Fig. 7. Illustration of two WGM sensor setups. (a) applying a tapped fiber; (b) applying an etched fiber. The evanescent field is introduced by total internal reflection of the light that propagating inside the fiber (shown as red lines).

Analytes measured by WGM sensors include BSA [7], DNA [6], bacteriorhodopsin [5], trypsin (via removal of BSA) [4], mercury [3], and thrombin [10]. A model system in which silica is etched off the surface of the resonator cavity and the WGM spectrum measured indicates the ability to detect sub-femtomole quantities of small molecules [8]. For bulk index change, a model system of ethanol and water indicate a resolution of approximately 10^{-7} RIU (refractive index unit) [2].

However, the use of a bare cavity WGM sensor requires intimate contact between the microresonator and an evanescent wave source, and precludes remote

sensing. The optical setup for this coupling is not mechanically stable due to the evanescent wave coupling. Thus, we seek to overcome this barrier by including a local source within the microresonator which will enable remote excitation of the sensor [13].

Weak modal structure has been observed from fluorescent dye/QD-embedded microspheres in water by laser trapping a sphere and simultaneously exciting the dye/QDs [9, 11]. The observed modal shift demonstrates the validity of the local source sensing approach. Functionality in such an aqueous environment is required for the sensing applications in this work. However, little attention has been paid to the microsphere size and the embedment of the QDs to the cavity in order to make the system suitable for sensing. By including local sources in the modal volume, i.e. near or on the outer surface of the microsphere, we can couple light into the resonant modes using a remote source to excite the local sources.

The repeatability of the systems depicted in Figure 7 strongly depends on the repeatability of the tunable laser, which is usually on the order of 0.1 nm, even though the linewidth of the laser line is only 0.1 pm. The system applying the broadband local source will not have the repeatability problem.

2.3 Quantum Dots

According to the previous section, an alternative method to couple the light into the microsphere employs an embedded light source. The method investigated in this work uses quantum dots (QDs) as the local source to couple in to WGMs.

Colloidal semiconductor quantum dots are single crystals that are a few nanometers in diameter. Absorption of a photon with energy above the semiconductor

band gap energy results in the creation of an electron-hole pair, which is also known as exciton. For nanocrystals smaller than the Bohr exciton radius (a few nanometers), energy levels are quantized, with values directly related to the size of QDs [27]. This effect is called quantum confinement as serves as the basis for the QD's unique optical properties. QDs have several advantages over organic fluorophores and have the potential to replace the organic dyes in many biological applications. The advantages include: broad absorption spectrum, photobleaching resistance, size-tunable absorption and emission spectra, and high quantum yield.

The absorption of QDs has an increased probability at higher energies and results in a broadband absorption spectrum [27]. QDs can be excited with simple excitation sources at essentially any wavelength from ultra-violet to the emission peak. This facilitates simultaneous excitation, detection, imaging and quantification of QDs. In the case of organic dyes, the emission and absorption peaks are close to each other. Though QDs have a smaller Stoke's shift than organic dyes, the broad absorption spectrum of QDs provides a large effective Stoke's shift.

The size of a QD is the dominant factor in determining the band gap, which can use to control its optical absorption and emission spectrum. The size of QDs can be precisely controlled by the duration, temperature, and ligand molecules used in the synthesis [27]. Thus, through size tunability, QDs can be fabricated to emit in a certain spectrum. This property of size tunability also makes QD's a good luminescence source for the sensor applications.

One of the main advantages of QDs is that they are highly photostable [28]. The reported comparison of photostability between CdSe/ZnS (core/shell) QDs to Alexa 488, which is one of the most photobleaching resistant dyes, shows the photostability of QDs are several magnitudes higher than organic dyes. In imaging and sensing applications, where a molecule has to be tracked for an extended period of time, photostability is the key factor. QDs are more suitable than the organic flurophores in our sensor setup.

Quantum yield is the ratio of the number of photons emitted to the number of photons absorbed. It has been found that the ZnS capped QDs can exhibit quantum yields close to 90% [27]. In the case for two photon excited luminescence, the action cross sections are the product of the nonlinear two-photon absorption cross section and the fluorescence quantum efficiency, and provide a direct measure of brightness for imaging. An action cross section of 47,000 GM is reported, which is two to three orders of magnitude larger than those of conventional fluorescent probes, and is an order of magnitude larger than those of organic molecules designed specifically for enhanced two-photon absorption [29].

2.4 Two-Photon Excitation Luminescence

Two-Photon Excitation (TPE) Luminescence is first predicted by Maria Goppert-Mayer in her 1931 doctoral dissertation [30]. The process that an atom or a molecule could absorb two photons simultaneously in the same quantum event was not confirmed until the early 1960's. TPE cross sections of different materials have since been determined [31].

When the photon density is very high, two photons can be absorbed simultaneously to the excited state. Because TPE is a second order nonlinear process, the emission intensity can be formulated by the following equation [31]:

$$I^{(2)} = \delta \int_{t=0}^{\infty} i(t)^2 \, dt \qquad (12)$$

Where δ is the TPE cross section. *i(t)* is the excitation light intensity. $I^{(2)}$ is the total power from the TPE luminescence. Denk et al. applied TPE luminescence to laser scanning microscopy [32]. The two photon laser scanning microscopy technique has many advantages over the conventional confocal luminescence microscopy. The primary advantage comes from the intrinsic localization of the TPE, as shown in Figure 8, thus provides better optical sectioning at greater depths in thick specimens.
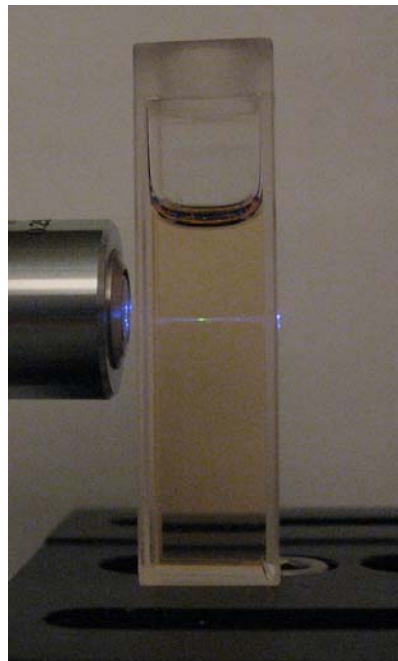
Fig. 8. Localized two-photon excitation. The luminescence from green QDs is induced by a focused femtosecond laser beam.

Since the probability of absorption decreases away from focus in TPE, more excitation light penetrates through a relatively thick specimen to the plane of focus. If we assume the beam has a Gaussian spatial profile, the excitation intensity with the volume of the focus decreases quadratically away from the focal volume. So the intensity from the TPE luminescence will decrease proportional to the forth order of the distance away from the focus plane. The well controlled TPE is well suited for our study of the localized coupling of the light into the microresonator.

3. METHODS AND MATERIALS

3.1 Sensor Element Parameter Design

According to previous section, the WGMs in microspheres can be theoretically

formulated by Mie theory. The resonance occurs when one of the eigen modes either TE

mode or TM mode dominates the scattering field.

Instead of running a full Mie code, which can be computationally intensive, there

are formulae that identify the low radial mode number resonance position, and linewidth

for bare spherical particles in free space derived from asymptotic formula of the explicit

Mie formalism [33]. To derive the formulae, the basic strategy is to express the spherical

Bessel functions as their asymptotic expansions, and apply the resonance condition (8a)

for TE modes and (8b) for TM modes to solve the equations.

For a WGM with the angular mode number l and radial mode number i, the

resonance size parameter is denoted as x^i_l. When the size parameter x is of several tens or

hundreds (which corresponds to a microsphere radius above 5 μm), the sphere size is

much larger than the wavelength in vacuum and the size parameter x^i_l can be

asymptotically expressed as the power expansion of $v^{1/3}$ [33].

$$
\begin{aligned}
mx^i_l = v &+ \frac{\alpha_i}{2^{1/3}} v^{1/3} - \frac{mp}{\sqrt{m^2-1}} + \frac{3\alpha_i}{10 \cdot 2^{2/3}} v^{-1/3} \\
&+ \frac{m^3 p(2p^2/3-1)\alpha_i}{2^{1/3}(m^2-1)^{3/2}} v^{-2/3} + O(v^{-1})
\end{aligned}
\tag{13}
$$

where $v = l+1/2$, p=1 for TE mode and p=1/m2 for TM mode. α_i is the *i*th zero of the

Airy function, For $l = 1, 2, 3$, α_i is 2.338, 4.088, and 5.521, respectively.

The corresponding FWHM in the certain resonance size parameter x is given by the following equation:

$$\Gamma_{l,i} = 2[N(x_l^i)^2 n_l^2 (x_l^i)]^{-1} \tag{14}$$

where n_l is the spherical Neumann function, and N is defined as follows:

$$N = m^2 - 1 \tag{15a}$$

$$N = (m^2 - 1)[\mu^2 + (\mu^2 / m^2 - 1)] \tag{15b}$$

where $\mu = v/x_l^i$, and equation (15a) is for TE modes, equation (15b) is for TM modes.

By differentiate the formula (1) we can derive the sensitivity as the following:

$$\left(\frac{\partial x_l^i}{\partial n_e}\right) = -\frac{1}{(m^2 - 1)^{3/2}}\left[1 + \frac{\alpha_i m^2}{2^{1/3}(m^2 - 1)} v^{-2/3}\right] \tag{16a}$$

$$\left(\frac{\partial x_l^i}{\partial n_e}\right) = -\frac{1}{m^2(m^2 - 1^2)^{3/2}}\left[(2m^2 - 1^2) + \frac{\alpha_i(2m^6 + m^4 - 4m^2 + 2)}{2^{1/3}m^2(m^2 - 1)} v^{-2/3}\right] \tag{16b}$$

where equation (16a) is for TE modes and equation (16b) is for TM modes.

The asymptotic expressions above are useful for sensor optimization design. The common materials for the microspheres are fused silica and polystyrene. The materials for the sensor are compared in terms of a sensor operating in water. In the calculation, the sphere radius is set to 5 μm. The refractive index of polystyrene is 1.591, and fused silica can be varied from 1.40 to 1.55. For this calculation, refractive index of fused silica $n_s = 1.47$ is used. Table 1 shows the calculated results.

Table 1 Theoretical calculations for microspheres. Theoretical Calculation: PS refractive index n_s=1.59, fused silica refractive index n_s=1.47, the immersion liquid is water n_e = 1.33. a, Microsphere radius; i, angular mode number; l, radial mode number; λ_{TE}, TE mode resonance wavelength, λ_{TM}, TM mode resonance wavelength, $\Delta\lambda= \lambda_{TE} - \lambda_{TM}$; Γ, the FWHM of the resonance peak.

Material	a (um)	i	l	λ_{TE} (nm)	λ_{TM} (nm)	$\Delta\lambda$ (nm)	Γ * (nm)	Sensitivity* (nm/RIU)
PS	5	1	84	549.77	546.96	2.81	0.095	33.7
Fused Silica	5	1	78	550.41	548.66	1.75	7.06	97.1
PS	5	2	78	549.23	546.83	2.40	4.69	40.1
Fused Silica	25	1	409	548.57	548.08	0.49	0.23e-5	14.6
Fused Silica	25	2	398	549.52	549.08	0.44	0.0024	16.5

* the terms are calculated for the TM modes.

The calculations indicate that the line widths for fused silica sphere are around 6nm, which is much broader than those of polystyrene sphere. The results also show that the peaks of the polystyrene sphere can be easily distinguished, for the distances between two adjacent modes of polystyrene sphere are around 3 nm, much larger than the line width of the peaks, which are around 0.08 nm. For fused silica sphere, the linewidths of the WGM peaks are larger than the distances between adjacent peaks. Thus the peaks are almost undistinguishable.

The effects of the radial number are also investigated. Within the same wavelength interval, the higher radial mode number corresponding to smaller angular mode number and results in broader linewidth. The calculation of the second radial modes in polystyrene sphere shows that the line widths are around 4 nm, which are around the same of the distances between adjacent modes. Thus, higher radial modes can not be observed effectively in the WGMs spectrum.

These effects are in agreement with the quantum analogy. For larger microspheres, the lower order angular modes are confined closer to the surface, and thus are more sensitive to the environmental change. Also for the same angular mode number, the larger radio number will have less confinement, so the linewidth will be broader and also have improved sensitivity.

For much larger spheres with radius around 25 μm, which are extensively used with end etched fiber with sweeping laser as the light source [2, 14], the linewidths for first radial modes are around 10^{-6} nm and the second radial modes are around 10pm. The large spheres required mechanism for very precise wavelength control, as reported using tunable laser source with 0.01 pm precision. Thus the large spheres are not suitable for the remote sensing with local broad band light source. In the end, we determined that polystyrene microsphere with a radius of 5 μm would be most appropriate for this application.

3.2 Sample Setup

QDs are embedded in the PS microspheres and serve as a local light source. As introduced in the previous section, compared to organic fluorescent dyes, QDs are much brighter and less susceptible to photobleaching. The QDs used in the experiments are CdSe cores with ZnS coating. The CdSe/Zns core/shell quantum dots are prepared colloidally via organometallic synthesis. In these experiments, green quantum dots with an emission peak at 530nm are used. The absorption and emission spectra are shown in Figure 9.
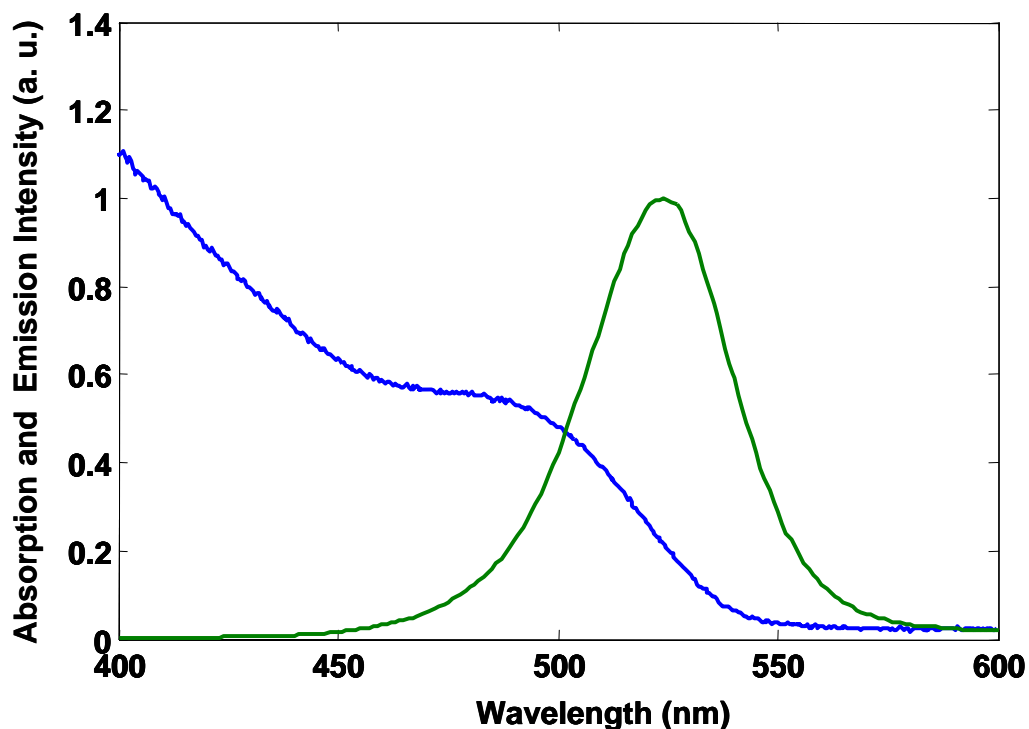
Fig. 9. Spectrum of quantum dots. The absorption (the blue line) and emission (the green line) curve of the green quantum dots for the experiments.

The polystyrene microspheres (Sulfate latex, Molecular Probes, Inc.) are infused with green CdSe/ZnS via diffusion. The microspheres have a mean radius of 4.8 μm and the standard deviation of size is 0.31 μm. The QDs are diffused into microspheres following reported methods.[34-36] Polystyrene can dissolve easily in chloroform but not in butanol. The microspheres are suspended in butanol and a suspension of CdSe/ZnS QDs in chloroform (concentration about 2.5 mg/L) added at a 19:1 volume ratio. The microspheres are partially swollen by chloroform and the QDs diffuse into the microspheres. After infusion at room temperature, the microspheres are re-suspended in butanol, and subsequently the QDs are captured inside of the subsurface area of the

microspheres. Figure 10 shows the confocal image of the QD-embedded microspheres. The detailed procedure is as follows:
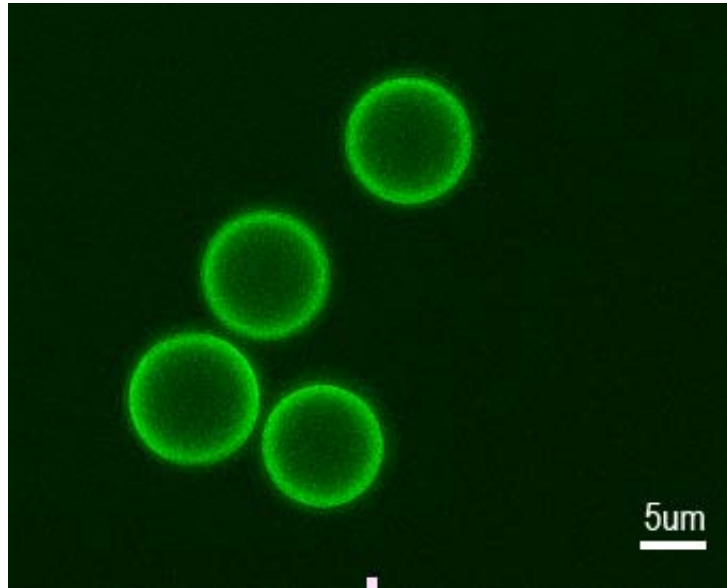
Fig. 10. Confocal image of QD embedded polystyrene microspheres.

1. Take PS spheres in water about 1.5 ml in a bullet;

2. centrifuge and pipette out water, then pipette in ethanol for three times;

3. centrifuge and pipette out ethanol, then pipette in butanol for three times;

4. at the fourth time, fill up only 1.0 ml butanol and put the QD/chloroform 0.25ml into the microsphere suspension;

5. let the QDs diffuse into the polystyrene microsphere suspension for one to four days (the longer the more QDs will diffuse into the microsphere).

6. pipette out the QD/chloroform/butanol mixture and fill up with butanol.

7. pipette out the butanol and fill with ethanol one time;

8. If needed, pipette out ethanol and suspend the spheres in water (DO NOT centrifuge this time, or the microspheres will be destroyed).

A thin film of polyethyleneimine (PEI) immobilizes the microspheres on a microscope cover slip, as shown in Figure 11. Due to the presence of surface sulfate group, the commercial plain polystyrene spheres usually have negative charge on the surface. Rinse the microscope slide cover slip several times and then drop 0.5 - 1 ml PEI to make a thin PEI film with diameter about 1.5 cm on the glass slide. Drop the microsphere in water suspension on the film. Because the PEI surface has positive charge, the microspheres are immobilized on the PEI thin film by electrostatic force. Rinse the cover slip two to three times to clean the microspheres that are not immobilized. The remaining microspheres are stable for the fluidic change during the experiments.
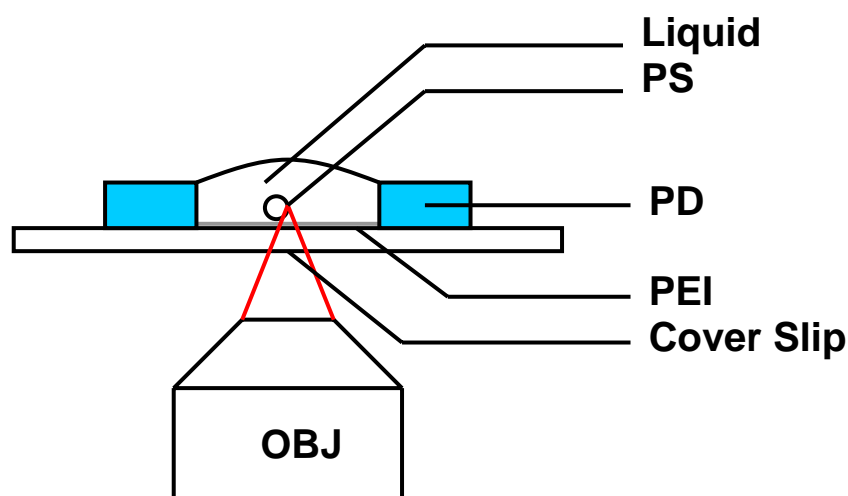

Fig. 11. Illustration of sample layout. PS, polystyrene microsphere; PD: Parafilm donut; PEI, PEI layer; Cover Slip, microscope cover slip.

3.3 Optical Setup

The experimental system layout is shown in Figure 12. The two-photon excitation light source used in the experiment is a Mira 900F pumped by a Verdi-V10 diode-pumped laser (Coherent Inc.), generating ~ 170 fs pulse with tunable central wavelength. A train of linearly polarized laser pulses reflected by a dichroic hot mirror with a cutoff wavelength at 650 nm are coupled into a long working distance microscope objective (Nikon 50X /0.85NA). The beam is focused onto a QD-embedded polystyrene microsphere on a microscope slide cover slip. Two linear polarizers are placed in front of the objective lens to control the power of the excitation laser beam. The angle of the second polarizer is fixed and the polarization of the light is not changed during the experiments. The luminescence from the quantum dot embedded polystyrene microspheres is collected by the same objective in reflection geometry. A 150 mm plano-covex lens serves as the tube lens to form a image to the spectrometer. A Schott color glass low pass filter (CVI laser, BG-39) is used to block the scattered excitation laser light. The spectrometer (PI-Acton SpectraPro 2300i, 750nm blazed 1200g/mm grating) with TE cooled CCD camera (PI-Acton, PIXIS 100) as the detector can operate in either imaging mode or spectrum collection mode. When operated in imaging mode, the grating is rotated so that the zero-order beam is imaged to the center of CCD camera and the slit opened to 2 mm corresponding to a field of view to about 40 μm. In spectrum collection mode, the slit width of 80 μm yields a wavelength resolution of 0.08 nm. A tungsten halogen lamp (Ocean Optics Inc. LS-1) is coupled into the optical fiber

as bright field illumination source. A condenser lens collimates the light out of the optical fiber onto the sample.
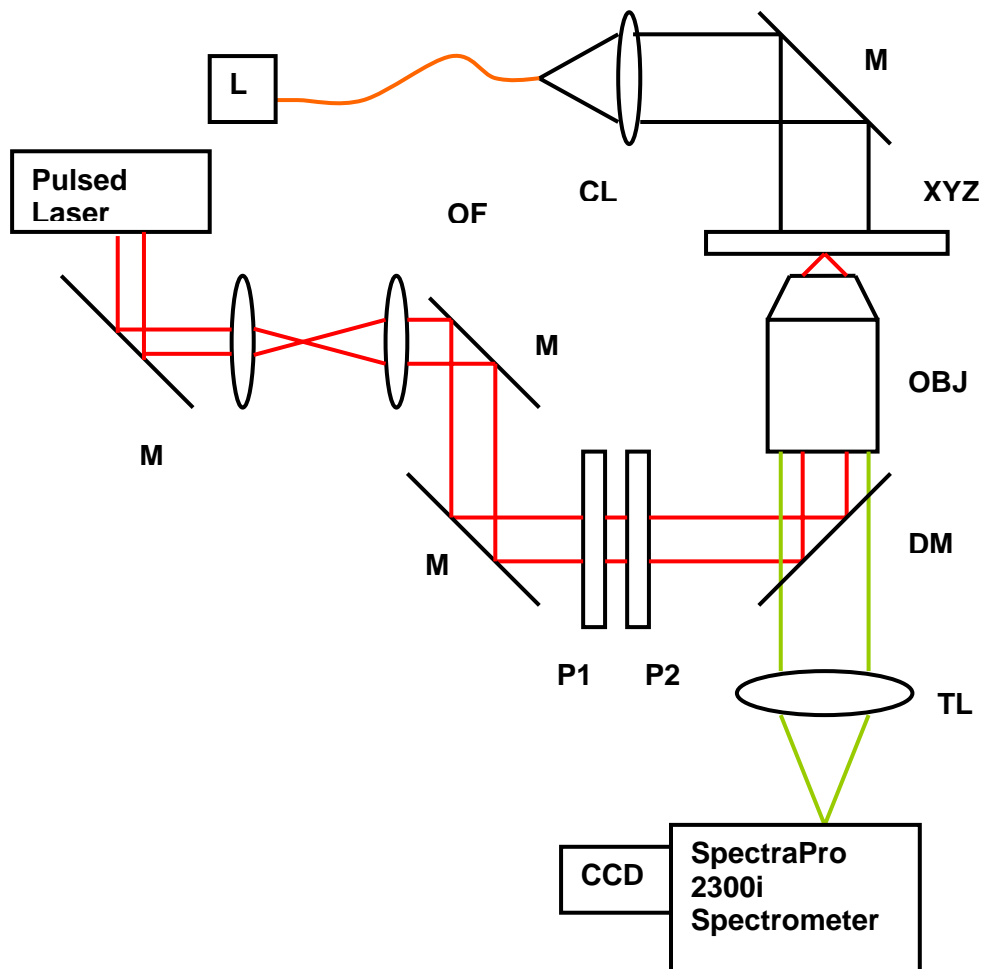

Fig. 12. Experimental setup. Pulsed Laser, Coherent Mira 900F; P1 and P2, polarizer; M, mirror; DM, dichroic Mirror; L, Ocean Optics tungsten halogen lamp; OBJ, objective Nikon 50X/0.85NA; TL, tube lens; XYZ, XYZ stage; CL, condenser lens; CCD, PI-Acton CCD spectrograph camera.

3.4 Experimental Procedure

Due to the localized nature of two-photon excitation, the position of coupling luminescence into microsphere WGMs can be well controlled. By placing the cover slip on an XYZ stage, the laser beam focus can be adjusted to any location within the microsphere. The relationship between the detection area and contrast of the resonance peak and luminescence from QDs will be studied.

Though WGMs are not surface modes, as discussed in previous section, the energy of the WGMs is localized in the near subsurface volume. Previous theoretical and experimental results have shown that for ideal coupling, the light source should coincide with the modal volume. For this reason, we focus the laser beam onto the lower part on the equator of the microsphere [37-39].

Two different microspheres are used in the refractive index sensor experiments. We select ethanol and water mixture as the immersion medium because the QD-embedded polystyrene microspheres are stable in an ethanol/water mixture, and also ethanol and water can be mixed at any ratio.

Microsphere 1: The refractive index of the immersion medium increases by adding ethanol into water. The refractive index can be determined by from the ratio of the mixture [40]. The QD-embedded microsphere is immersed in:

(a) pure water, $n_e = 1.333$;

(b) 15.2% ethanol water mixture, $n_e = 1.343$;

(c) 27.9% ethanol water mixture, $n_e = 1.352$;

(d) 52.0% ethanol water mixture, $n_e = 1.362$.

Microsphere 2: The refractive index of the immersion medium decreases by adding ethanol water mixture of different ratio. Each mixture is added separately, and removed before the next experiment. The QD-embedded microspheres are immersed in:

(a) ethanol $n_e = 1.363$;

(b) ~40% ethanol water mixture;

(c) ~20% ethanol water mixture;

In all the experiments, the central wavelength of the laser is tuned to 800 nm, and the excitation is maintained at 17 mW.

4. RESULTS

4.1 Visibility

Figure 13(a) shows a bright field image of an immobilized microsphere in water from our experiment setup. Figure 13(b) shows the dark field image of the QD-embedded microsphere when the focus of the laser is adjusted to the lower part of the microsphere on the equator plane. Two locations with highest luminescent intensity can be easily distinguished. One position is at the excitation position as shown with the circle in figure 13(b). The other is at the opposite point to the excitation point.
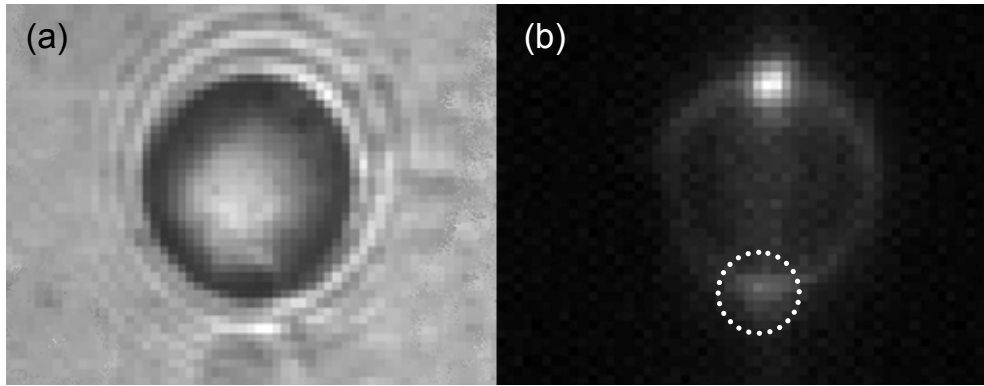
Fig. 13. A immobilized QD-embeded PS microsphere. (a) bright field image; (b) dark field image when QDs are locally excited at the lower portion of the microsphere. The area highlighted by the dotted circle is the excitation location.

In order to quantify the contrast of the WGM peaks to the quantum dots background luminescence, the visibility V is defined as $V = (I_{peak} - I_{background})/(I_{peak} + I_{background})$ [38, 41]. The luminescence spectrum of the QD-embedded microsphere over the whole area on the CCD detector is compared to that only from the area opposite to the excitation, as shown in Fig. 14. The visibility of the resonance from the

luminescence from the whole area is 0.24, and the visibility of the resonance from only the other maximum is 0.76. The enhancement of the visibility is over three times.

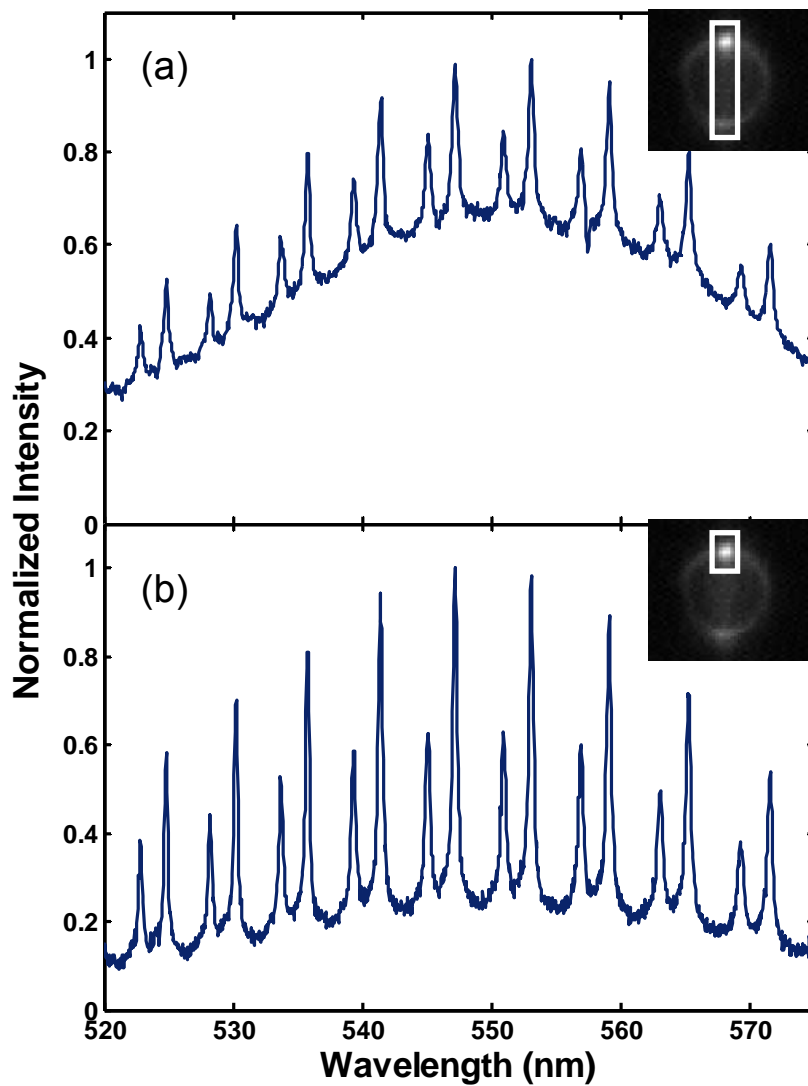Fig. 14. Visibility of different detection location. (a) the WGMs spectrum over the entire area; (b), the WGMs spectrum at only the area the upper portion of the QD-embedded microsphere. The there times of visibility enhancement is observed.

4.2 Resonance Shift due to Refractive Index Change

Table 2 and table 3 show the wavelength of the WGM peaks from Microsphere1 and Microsphere 2, respectively. Figure 15 and figure 16 shows the WGM spectra of Microsphere 1 and Microsphere 2, respectively. The spectra clearly show several pairs of TE and TM peaks across the detection range. Both microspheres show that when the refractive index of the immersion medium increases, the WGM peaks will shift to longer wavelength. The broadening effect of the WGM peaks from a low refractive index medium to a high refractive index medium is also observed.

From the calculation of the spacing between adjacent modes, we conclude that the WGM peaks with higher intensity of each TE/TM pair are TE modes, and the ones with lower intensity are TM modes. This can also be verified by the fact that the shift the TM mode is larger than that of the TE mode of the same quantum number. In agreement with the theoretical calculation, the results show that the TM modes have broader linewidths than that of TE modes with the same mode number.

Table 2 The WGM peaks of Microsphere 1.

Water n_e = 1.333		n_e = 1.343		n_e = 1.352		n_e = 1.362	
TM	TE	TM	TE	TM	TE	TM	TE
523.03	525.27	524.76	526.85	526.06	528.15	527.64	529.68
528.8*	531.03*	530.47*	532.6*	531.91*	533.94*	533.62*	535.55*
534.59	542.9	536.24	544.49	537.76	545.91	539.28	547.41
546.59	548.96	548.36	550.63	549.86	552.04	551.59	553.62
552.81	555.2	554.57	556.91	556.15	558.35	557.86	559.92
559.16*	561.67*	561.04*	563.32*	562.52*	564.8*	564.35*	566.45*
565.69	568.18	567.47	569.91	569.07	571.42	570.84	573.1

* are the data that marked by the arrows in figure 15 and for sensitivity calculation

Table 3 The WGM peaks of Microsphere 2.

Ethanol $n_e = 1.363$		$n_e \approx 1.357$**		$n_e \approx 1.345$**	
TM modes	TE modes	TM modes	TE modes	TM modes	TE modes
525.61	527.51	524.67	526.63	522.81	524.81
531.17*	532.98*	530.16*	532.10*	528.21*	530.20*
536.53	538.55	535.70	537.58	533.67	535.74
542.21	544.13	541.39	543.31	539.33	541.39
547.96	550.04	547.14	549.09	545.09	547.18
554.02	555.87	553.03	555.02	550.95	553.08
560.01*	561.93*	559.06*	561.13*	556.91*	559.11*
566.13	568.08	565.19	567.28	563.05	565.28
572.29	547.64	571.54	573.57	569.24	571.58

* are the data that are used for sensitivity calculation. ** The exact refractive indices are unknown; the error could be on the order of 0.005 RIU.

The sensitivities of the shifts of Microsphere 1 for the four WGMs in figure 15 marked as TM a, TE a, TM a-5 and TE a-5modes are 166 nm/RIU (refractive index units), 155 nm/RIU, 178 nm/RIU and 170 nm/RIU, respectively. Because the process of decreasing the refractive index can not be as well controlled as increasing the refractive index by adding ethanol into water, the exact refractive index is difficult to estimate. The sensitivities of the shifts of Microsphere 2 for the four WGM peaks are estimated as 164 nm/RIU, 154 nm/RIU, 172nm/RIU, 156nm/RIU [13]. The main purpose for Microsphere 2 is to serve as a reference data to ensure the response is not dependent on the direction of the refractive index change.

Fig. 15. WGM spectra from Microsphere 1. The microsphere is in ethanol water mixtures of different ratios by weight: (a) 52.0% ethanol water mixture, ne = 1.3621; (b) 27.9% ethanol water mixture, ne = 1.3522; (c) 15.2% ethanol water mixture, ne = 1.3434; and (d) pure water, ne= 1.3330. The solid arrows represent TM modes, and the dotted arrows represent TE modes.
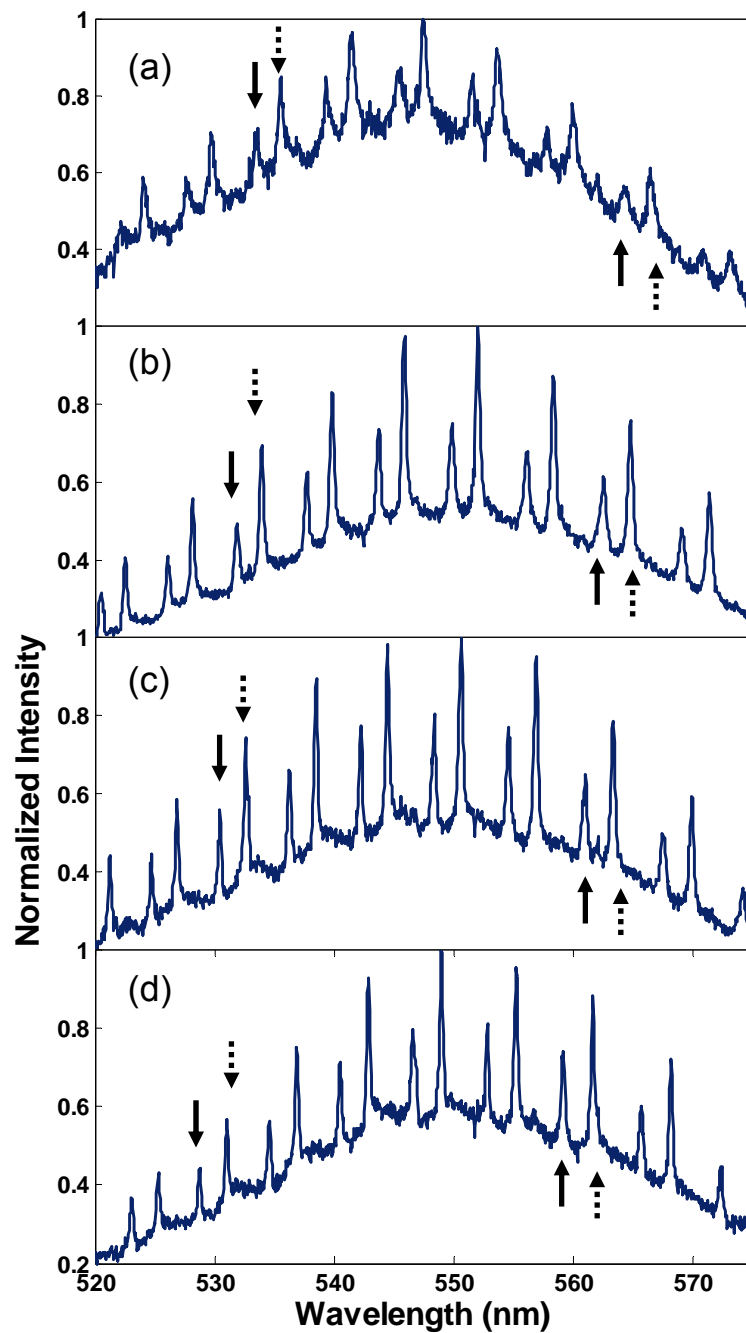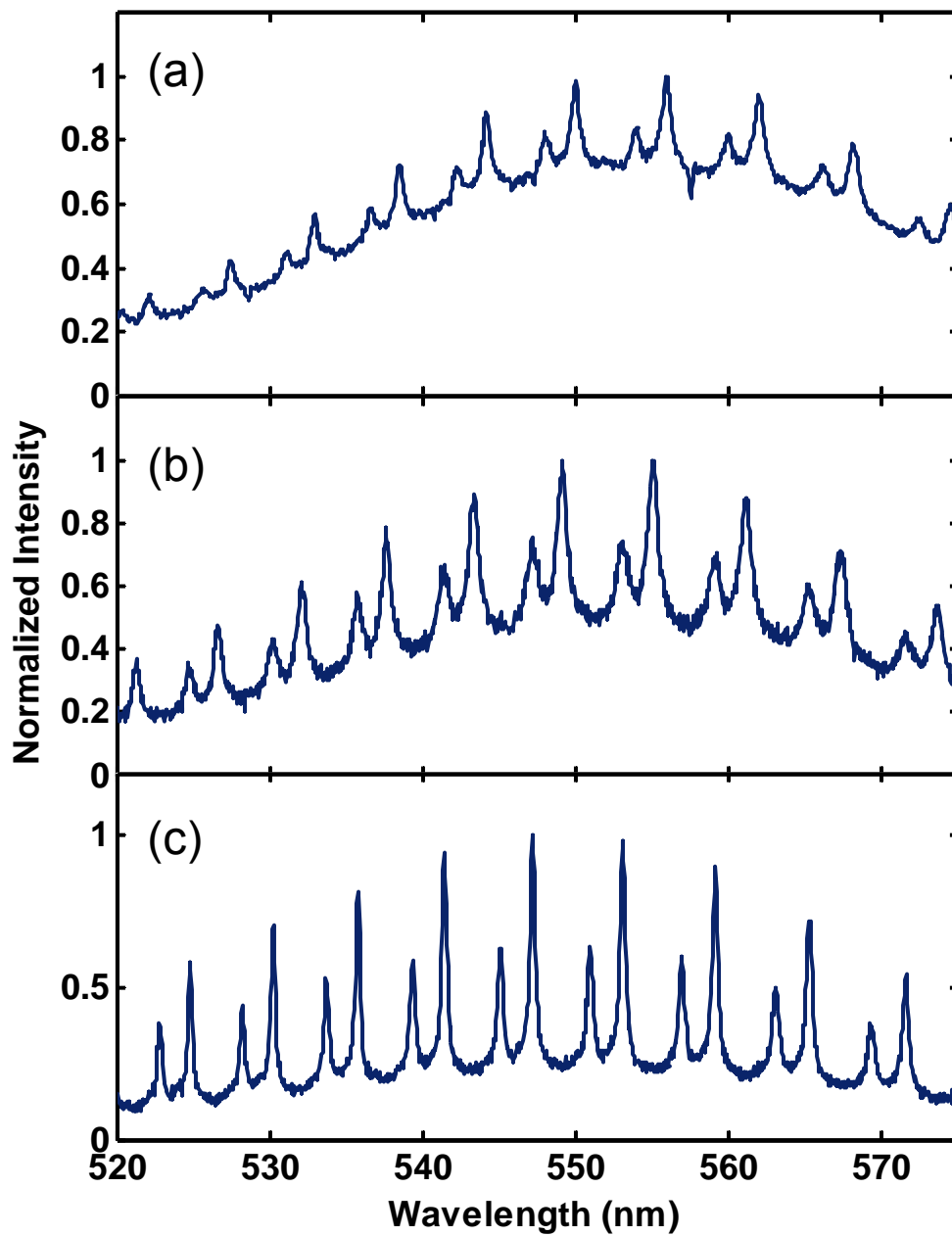
Fig. 16. WGM spectra from Microsphere 2. The microsphere is in ethanol water mixtures of different ratios by weight: (a) ethanol ne = 1.363; (b) ~40% ethanol water mixture; (c) ~20% ethanol water mixture.

5. DISCUSSION

In previous work, the multiple multipole (MPM) technique was used to calculate the electromagnetic field distribution of a single mode. The results showed that the intensity of the WGM will have a maximum spot opposite to the dipole [37, 39]. In the experiment, the observed intensity distribution is contributed to by all resonance modes within the microsphere. So the two maxima at the excitation and the opposite location can be easily distinguished, which is in agreement with the experimental observation.

Because WGMs result from the total internal reflection of the light along the spherical surface, and due to the nature of the luminescence from the QDs, only a portion of the light can be coupled into the microcavity and contribute to the WGMs. As a result, the resonance component of the spectrum of the location opposite to the excitation should be greater than that from the excitation location.

According to equation (13) for the same refractive index change of the environmental liquid, the resonance peak with a smaller size parameter will have a larger spectral shift, while the resonance peak with larger size parameter will provide smaller FWHM, i.e. sharper peaks. Also for the same angular mode number, the resonance with larger radial mode number will have a larger FWHM. In our experiments only the first radial modes are considered.
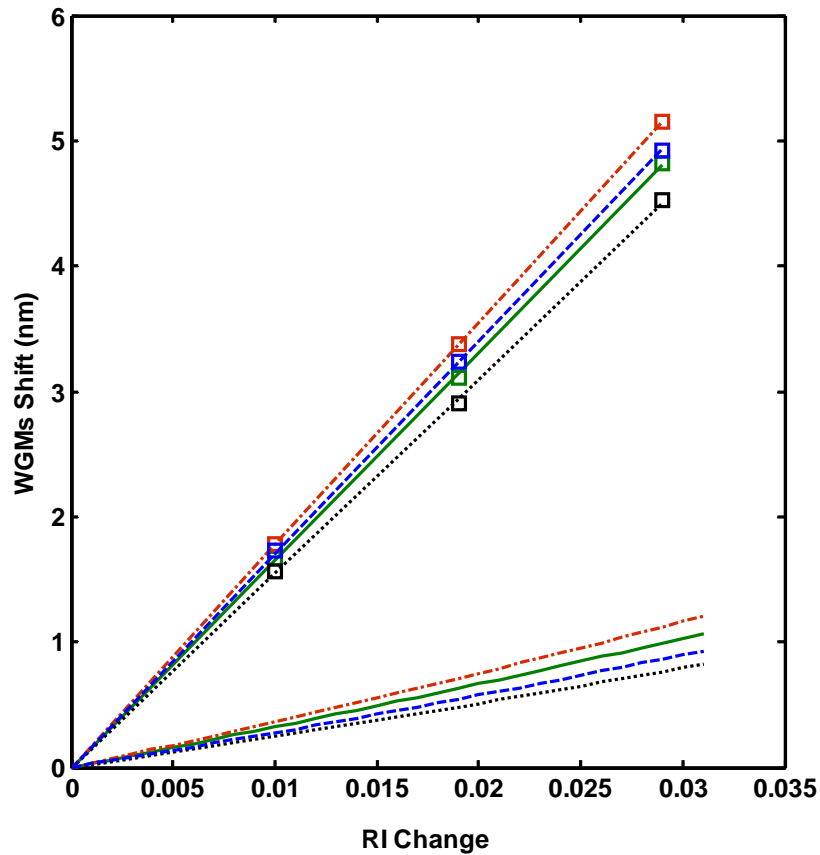
Fig. 17. Sensitivity of the WGM sensor. The experimental and theoretical sensitivity of WGM sensor. The sensitivities of the shifts for the four WGMs in figure 15 marked as TM a, TE a, TM a-5 and TE a-5 modes with a radius of 5 μm for TM 88 (green), TE 88 (black), TM 83 (red) and TE 83 (blue) modes.

Because the exact size of microspheres is unknown, instead of assigning exact mode number to these modes we denote the four WGM peaks marked in figure 15 as TM a, TE a, TM a-5 and TE a-5. The sensitivities of the WGMs shifts are 165.6 nm/RIU, 155.2 nm/RIU, 177.7 nm/RIU and 170.1 nm/RIU, respectively. The theoretical WGM sensitivities of a polystyrene microresonator with a radius of 5 μm for TM 88, TE 88, TM 83 and TE 83 modes give a close match for the experimental results (the peaks are at 523.3 nm, 525.9 nm, 553.2 nm, and 556.1 nm in water). The theoretical sensitivities for

the modes in bare microsphere are 32.3 nm/RIU, 24.9 nm/RIU, 38.6 nm/RIU, and 28.1 nm/RIU respectively. Figure 17 plots the shifts of the experimental results and the calculated sensitivity. About a five fold enhancement of sensitivity is observed.

The sensitivity enhancement may result from the embedded CdSe/ZnS (n=2.45) QD layer. As has been shown theoretically [42, 43] and experimentally [44], a high refractive index layer will move the confinement of the WGM energy closer to the surface and yield resonance modes more sensitive to refractive index changes.

As the quantum mechanics analogy shows, the potential function for a coated microsphere can be expressed as [42-44]:

$$V_l(r) = \begin{cases} k^2(1-m_1^2)+l(l+1)/r^2, \text{ for } r \leq (a-t) \\ k^2(1-m_2^2)+l(l+1)/r^2, \text{ for } (a-t) < r \leq a \\ l(l+1)/r^2, \text{ for } a < r \end{cases} \qquad (17)$$

where t is the thickness of the layer; m_1 and m_2 is the refractive index of the core and the coating, respectively. Figure 18 plots the potential function for a core refractive index of 1.59, coating refractive index of 2.00 in air. The ratio of thickness of the shell to the whole radius is 1/100.

Because the diffusion of the QDs is a passive process, and only the surface of the polystyrene is swollen, the QD layer should be less than a few diameters of the QDs. Also from the confocal image (figure 7) of the microsphere, the QD layer is less than the resolution of the confocal microscope; about 122 nm. For this thickness, the QD-embedded layer will not move the confinement out of the polystyrene core and thus will not significantly shift the modal position. However due to the spatial modal location

being closer to the surface, the modes will be more sensitive to refractive index changes. In other words, the "dip" of the potential well is not "wide" enough to trap the peak of the energy into the coated layer, so the proposed enhancement could be as high as we observed in the experiments.
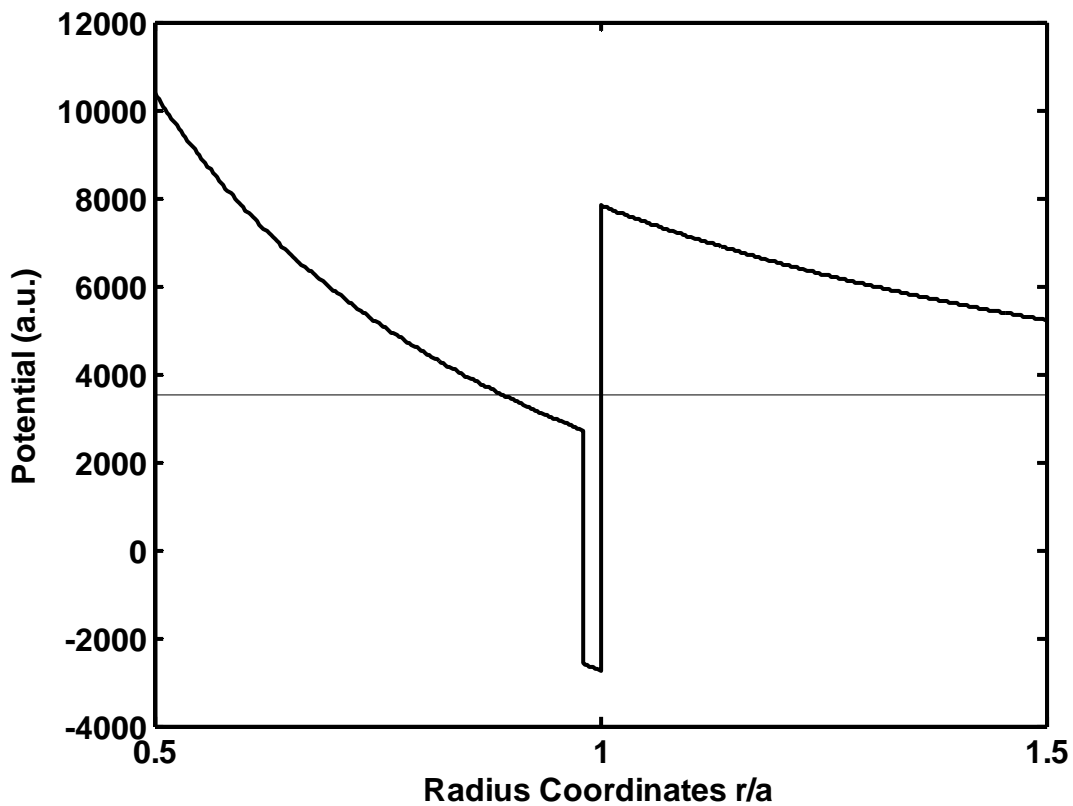
Fig. 18. Effective potential function for a coated microsphere. Low refractive index microsphere (n = 1.59) coated with a high refractive index layer (n = 2.0).

If the peak of energy of the WGMs move into the coated layer, the effect of the potential well is more like a bare microsphere with a refractive index as the coating material, and the enhancement effect will not be very significant. From the experimental results, we also observed a decrease of the ratio of sensitivity of TE/TM modes.

According to the same reference, this is also an indication that the peak of the energy is still within the core of the microsphere. Nevertheless, the full effects of the QD layer are under continued investigation.

The characterization of multiple WGM shifts improves the estimation of the refractive index change compared to a single WGM shift. By linearly fitting the shift of each WGM independently, the fitted refractive indices of the immersion medium are calculated from each line function. The averages of the fitted refractive index changes from water to the water/ethanol mixtures for all 14 modes are 0.0102, 0.0190, and 0.0289 and the standard deviations are 2.2×10^{-4}, 1.9×10^{-4}, and 1.3×10^{-4} respectively. With an equivalent wavelength pitch of 0.04 nm and the sensor element sensitivity of about 160 nm/RIU, the minimum detectable refractive index change can be estimated as 2.5×10^{-4} RIU. The standard deviations of the fitted refractive indices are less than the minimum detectable refractive index change limited by the spectrometer. Thus, the pitch between two adjacent CCD pixels is the major limitation of the sensor system.

Though the detection limit of our system is lower than the reported WGM sensors based on large spheres, the sensitivity of our sensor elements is actually ten times higher than that of other systems. If the detection limit of the resonance shifts can be improved to 0.1 pm, a detection limit on the order of 10^{-7} RIU can be achieved.

6. SUMMARY

In summary, this thesis demonstrates a tagless remote refractometric sensor based on WGMs in a QD-embedded microsphere. The QD's luminescence acts as a local broadband light source. QDs, which have higher quantum yield and better resistance to photo bleaching, are able to provide a stronger and stable signal for this sensor application. The spatial intensity distribution of WGMs is observed by applying a femtosecond laser to induce localized two-photon excitation. An improved peak to background ratio was achieved by selecting the detection position. We measure the WGMs shifting as the refractive index of the immersion fluid change. About five times of enhancement of the sensitivity over the theoretical calculation in uncoated microspheres is observed. By averaging the relative shift of all the modes within the quantum dot emission spectrum, higher accuracy of refractive index can be achieved than focusing on only one mode. The improved sensitivity and accuracy of WGM based refractometric sensors offer a promising opportunity for development of optoelectronic devices for bio-application.

There are two further directions for this project:

1. The application of the sensor unit to biochemical sensing. The surface of the polystyrene microsphere can be functionalized for glucose sensing. The surface group of the QDs can also be applied for specific chemical sensing.

2. The improvement of the detection of the wavelength shift. One of the feasible methods using the intensity difference between adjacent pixels to realize sub picometer wavelength shift detection [45].

REFERENCES

1.   A. M. Armani, R. P. Kulkarni, S. E. Fraser, R. C. Flagan, and K. J. Vahala, "Label-free, single-molecule detection with optical microcavities," Science **317**, 783-787 (2007).

2.   N. M. Hanumegowda, C. J. Stica, B. C. Patel, I. White, and X. D. Fan, "Refractometric sensors based on microsphere resonators," Applied Physics Letters **87**, 201107 (2005).

3.   N. M. Hanumegowda, I. M. White, and X. D. Fan, "Aqueous mercuric ion detection with microsphere optical ring resonator sensors," Sensors and Actuators B-Chemical **120**, 207-212 (2006).

4.   N. M. Hanumegowda, I. M. White, H. Oveys, and X. D. Fan, "Label-free protease sensors based on optical microsphere resonators," Sensor Letters **3**, 315-319 (2005).

5.   J. Topolancik, and F. Vollmer, "Photoinduced transformations in bacteriorhodopsin membrane monitored with optical microcavities," Biophysical Journal **92**, 2223-2229 (2007).

6.   F. Vollmer, S. Arnold, D. Braun, I. Teraoka, and A. Libchaber, "Multiplexed DNA quantification by spectroscopic shift of two microsphere cavities," Biophysical Journal **85**, 1974-1979 (2003).

7.   F. Vollmer, D. Braun, A. Libchaber, M. Khoshsima, I. Teraoka, and S. Arnold, "Protein detection by optical shift of a resonant microcavity," Applied Physics Letters **80**, 4057-4059 (2002).

8.   I. M. White, N. M. Hanumegowda, and X. D. Fan, "Subfemtomole detection of small molecules with microsphere sensors," Optics Letters **30**, 3189-3191 (2005).

9.   L. M. Zhang, Y. X. Wang, F. J. Zhang, and R. O. Claus, "Observation of whispering-gallery and directional resonant laser emission in ellipsoidal microcavities," Journal of the Optical Society of America B: Optical Physics **23**, 1793-1800 (2006).

10.   H. Y. Zhu, J. D. Suter, I. M. White, and X. D. Fan, "Aptamer based microsphere biosensor for thrombin detection," Sensors **6**, 785-795 (2006).

11.   P. Zijlstra, K. L. van der Molen, and A. P. Mosk, "Spatial refractive index sensor using whispering gallery modes in an optically trapped microsphere," Applied Physics Letters **90**, 161101 (2007).

12.   M. A. van Dijk, L. C. Kapitein, J. van Mameren, C. F. Schmidt, and E. J. G. Peterman, "Combining optical trapping and single-molecule fluorescence spectroscopy: enhanced photobleaching of fluorophores," J. Phys. Chem. B **108**, 6479-6484 (2004).

13.   S. Pang, R. E. Beckham, and K. E. Meissner, "Quantum dot-embedded microspheres for remote refractive index sensing," Applied Physics Letters **92**, 221108 (2008).

14.   S. Pang, and K. Meissner, "Tagless remote refractometric sensor based on WGMs in quantum dot-embedded microspheres," Proceedings of SPIE **6863**, 686303 (2008).

15.   B. R. Johnson, "Theory of morphology-dependent resonances - shape resonances and width formulas," Journal of the Optical Society of America A-Optics Image Science and Vision **10**, 343-352 (1993).

16.   C. F. Bohren, and D. R. Huffman, *Absorption and Scattering of Light by Small Particles* (Wiley, New York, 1998).

17.   J. R. Probertjones, "Resonance Component of Backscattering by Large Dielectric Spheres," Journal of the Optical Society of America a-Optics Image Science and Vision **1**, 822-830 (1984).

18.   L. Rayleigh, "The problem of the whispering gallery," Philosophical Magazine **20**, 1001-1004 (1910).

19.   I. Teraoka, and S. Arnold, "Theory of resonance shifts in TE and TM whispering gallery modes by nonradial perturbations for sensing applications," Journal of the Optical Society of America B-Optical Physics **23**, 1381-1389 (2006).

20.   I. Teraoka, S. Arnold, and F. Vollmer, "Perturbation approach to resonance shifts of whispering-gallery modes in a dielectric microsphere as a probe of a surrounding medium," Journal of the Optical Society of America B-Optical Physics **20**, 1937-1946 (2003).

21.   W. P. Ambrose, P. M. Goodwin, and J. P. Nolan, "Single-molecule detection with total internal reflection excitation: Comparing signal-to-background and total signals in different geometries," Cytometry **36**, 224-231 (1999).

22.   T. Funatsu, Y. Harada, M. Tokunaga, K. Saito, and T. Yanagida, "Imaging of single fluorescent molecules and individual ATP turnovers by single myosin molecules in aqueous solution," Nature **374**, 555-559 (1995).

23.   B. D. Moore, L. Stevenson, A. Watt, S. Flitsch, N. J. Turner, C. Cassidy, and D. Graham, "Rapid and ultra-sensitive determination of enzyme activities using surface-enhanced resonance Raman scattering," Nature Biotechnology **22**, 1133-1138 (2004).

24.   R. C. Hughes, A. J. Ricco, M. A. Butler, and S. J. Martin, "Chemical microsensors," Science **254**, 74-80 (1991).

25.   Z. H. Zhong, D. L. Wang, Y. Cui, M. W. Bockrath, and C. M. Lieber, "Nanowire crossbar arrays as address decoders for integrated nanosystems," Science **302**, 1377-1379 (2003).

26.   J. M. Nam, C. S. Thaxton, and C. A. Mirkin, "Nanoparticle-based bio-bar codes for the ultrasensitive detection of proteins," Science **301**, 1884-1886 (2003).

27.   X. Michalet, F. F. Pinaud, L. A. Bentolila, J. M. Tsay, S. Doose, J. J. Li, G. Sundaresan, A. M. Wu, S. S. Gambhir, and S. Weiss, "Quantum dots for live cells, in vivo imaging, and diagnostics," Science **307**, 538-544 (2005).

28.   X. Y. Wu, H. J. Liu, J. Q. Liu, K. N. Haley, J. A. Treadway, J. P. Larson, N. F. Ge, F. Peale, and M. P. Bruchez, "Immunofluorescent labeling of cancer marker Her2 and other cellular targets with semiconductor quantum dots," Nature Biotechnology **21**, 452-452 (2003).

29.   D. R. Larson, W. R. Zipfel, R. M. Williams, S. W. Clark, M. P. Bruchez, F. W. Wise, and W. W. Webb, "Water-soluble quantum dots for multiphoton fluorescence imaging in vivo," Science **300**, 1434-1436 (2003).

30.   M. Goepert-Mayer, "Ueber Elementarakte mit zwei Quantenspruengen," Annalen der Physik **401**, 273-294 (1931).

31.   C. Xu, W. Zipfel, J. B. Shear, R. M. Williams, and W. W. Webb, "Multiphoton fluorescence excitation: New spectral windows for biological nonlinear microscopy," Proceedings of the National Academy of Sciences of the United States of America **93**, 10763-10768 (1996).

32.   W. Denk, J. H. Strickler, and W. W. Webb, "Two-photon laser scanning fluorescence microscopy," Science **248**, 73-76 (1990).

33.   C. C. Lam, P. T. Leung, and K. Young, "Explicit asymptotic formulas for the positions, widths, and strengths of resonances in Mie scattering," Journal of the Optical Society of America B-Optical Physics **9**, 1585-1592 (1992).

34.   W. N. Everett, R. E. Beckham, K. Meissner, and M. A. Bevan, "Evanescent wave excited luminescence from levitated quantum dot modified colloids," Langmuir **23**, 8950-8956 (2007).

35.   Z. A. Peng, and X. Peng, "Formation of high-quality CdTe, CdSe, and CdS nanocrystals using CdO as precursor," Journal of American Chemical Society **123**, 183-184 (2001).

36.   K. E. Meissner, E. Herz, R. P. Kruzelock, and J. W. B. Spillman, "Quantum dot-tagged microspheres for fluid-based DNA microarrays," Physica Status Solidi (c) **0**, 1355-1359 (2003).

37.   B. M. Moller, U. Woggon, M. V. Artemyev, and R. Wannemacher, "Photonic molecules doped with semiconductor nanocrystals," Physical Review B **70**, 115323 (2004).

38.   D. Morrish, X. S. Gan, and M. Gu, "Morphology-dependent resonance induced by two-photon excitation in a micro-sphere trapped by a femtosecond pulsed laser," Optics Express **12**, 4198-4202 (2004).

39.   U. Woggon, R. Wannemacher, M. V. Artemyev, B. Moller, N. Lethomas, V. Anikeyev, and O. Schops, "Dot-in-a-dot: electronic and photonic confinement in all three dimensions," Applied Physics B **77**, 469-484 (2003).

40.   W. R. Veazey, C. D. Hodgman, and Chemical Rubber Company., *Handbook of Chemistry and Physics*, (Chemical Rubber Pub. Co., Cleveland, 1980).

41.   D. M. Morrish, X. S. Gan, and M. Gu, "Observation of orthogonally polarized transverse electric and transverse magnetic oscillation modes in a microcavity excited by localized two-photon absorption," Applied Physics Letters **81**, 5132-5134 (2002).

42.   I. Teraoka, and S. Arnold, "Enhancing the sensitivity of a whispering-gallery mode microsphere sensor by a high-refractive-index surface layer," Journal of the Optical Society of America B-Optical Physics **23**, 1434-1441 (2006).

43.   I. Teraoka, and S. Arnold, "Whispering-gallery modes in a microsphere coated with a high-refractive index layer: polarization-dependent sensitivity enhancement of the resonance-shift and TE-TM resonance matching," Journal of the Optical Society of America B-Optical Physics **24**, 653-659 (2007).

44.   O. Gaathon, J. Culic-Viskota, M. Mihnev, I. Teraoka, and S. Arnold, "Enhancing sensitivity of a whispering gallery mode biosensor by subwavelength confinement," Applied Physics Letters **89**, 223901 (2006).

45.	O. Schmidt, P. Kiesel, S. Mohta, and N. M. Johnson, "Resolving pm wavelength shifts in optical sensing," Applied Physics B-Lasers and Optics **86**, 593-600 (2007).

VITA

Name:	Shuo Pang
Address:	3120 TAMU
	Room 337 Zachry Engineering Center
	College Station, TX 77843
Email Address:	shuopang02@yahoo.com
Education:	B.E. Mechanical Engineering, Tsinghua University, Jul. 2006.
	M.S. Biomedical Engineering, Texas A&M University, Aug. 2006